Received: 11 March 2019 | Revised: 13 April 2019 | Accepted: 19 April 2019

DOI: 10.1002/aoc.4987

FULL PAPER

WILEY Applied Organometallic Chemistry

Sulfonated salicylidene thiadiazole complexes with Co (II) and Ni (II) ions as sustainable corrosion inhibitors and catalysts for cross coupling reaction

Hany M. Abd El-Lateef[1,2] | Abdelwahed R. Sayed[1,3] | Mohamed Shaker S. Adam[1,2]

[1] Department of Chemistry, College of Science, King Faisal University, P.O. Box 380, Al Hufuf 31982Al Hassa, Saudi Arabia

[2] Chemistry Department, Faculty of Science, Sohag University, Sohag 82534, Egypt

[3] Department of Chemistry, Faculty of Science, University of Beni Suef, Egypt

Correspondence
Hany M. Abd El-Lateef and Mohamed Shaker S. Adam, Department of Chemistry, College of Science, King Faisal University, P.O. Box 380 Al Hufuf 31982 Al Hassa, Saudi Arabia.
Email: hmahmed@kfu.edu.sa; hany_shubra@yahoo.co.uk; madam@kfu.edu.sa

Funding information
Deanship of Scientific Research, King Faisal University, Grant/Award Number: 180084

Condensation of 2,5-dihydrazinyl thiadiazole with 5-sodium sulfonate salicylaldehyde afforded dibasic tetradentate pincer *N,O,O,N*-salicyldiene thiadiazole ligand (H_2Sanp). The novel dipolar ligand formed para-magnetic pincer complexes within Co (II) and Ni (II) ions (Co-Sanp and Ni-Sanp) under sustainable conditions. The water-soluble ligand and its metal-complexes were estimated by mass, IR and UV–Visible spectroscopy, EA (elemental analyses), TGA (Thermogravimetric analyses), magnetic susceptibility, and conductivity measurements. The catalytic reactivity of Co-Sanp and Ni-Sanp were evaluated in the Suzuki and Buchwald-Hartwig cross coupling reaction in aqueous-methanol binary mixtures. Both reactions of boronic acid or aryl amines with aryl halides gave high chemoselective yield of C—C or C—N product. The inhibition characteristics of H_2Sanp and its Ni- and Co-complexes were performed for the C-steel corrosion in 1.0 M HCl using electrochemical measurements and surface analysis methods. These methods indicated that the synthesized compounds have served as efficient mixed-type corrosion inhibitors and their adsorption on the steel surface obeyed isotherm model of Langmuir. Co-Sanp inhibitor displays the best corrosion inhibition efficiency, and the capacity is up to 97.11% at of 250 mg L^{-1}. Surface analysis confirms formation of protective layer on the C-steel surface.

KEYWORDS
catalysis, complexes, corrosion protection, Thiadiazole dihydrazone

1 | INTRODUCTION

Thiadiazoles are substantial class of heterocyclic compounds with comprehensive framework of biological accomplishments and applicability in parts of polymer pharmaceutical, agricultural chemistry, industrial, bactericides, herbicides, fungicides and regulators of plant growth.[1] Structure and synthesis of 2,5-dihydrazino-1,3,4-thiadiazole and its derivatives was reported previously.[2] Reactivity of hydrazonoyl halides towards 2,5-dihydrazinyl-1,3,4-thiadiazole gives bis-triazines holding thiadiazole, while the reactivity of 2,5-dihydrazinyl-1,3,4-thiadiazole to the active methylene reagents afforded pyrazoles of thiadiazole derivatives.[3,4]

One of the most versatile and prevalent recent synthetic devises is cross coupling reactions within constructing of C—C and C—N bonding of organic chains[5] with wide and high utility in synthesis of large number of organic compounds, which are applicable in manufacturing and as pharmaceuticals.[6,7] Despite, palladium complexes are the most effective catalysts for cross coupling reactions with high selectivity and low by-products,[8] nickel and cobalt pincer complexes compete for that propose due to their low cost, high abundance in earth crust, easily handled, and high stable.[9] For that, recent catalytic cross coupling reactions were achieved by many 3d transition metal complexes, e.g. Ni (II) and Co (II), homogeneously[10–12] and heterogeneously.[13,14] Indeed, nickel pincer chelates could be regarded as effective catalysts for cross-couplings of various organometallic substrates with organic halides demonstrate high potential with respect to palladium ones.[15]

High coordination behavior of cheap N^O, as hard donor ligands, *e.g.* Schiff bases, towards transition metal ions of various oxidation states, attracted inorganic chemists to apply such complexes as effective catalysts in cross coupling processes.[16] Cross couplings catalyzed by Cobalt (II) chelates are interesting search point in organic syntheses,[17] which highly developed in last decade.[18] Singh *et al*. incorporated new Co (II), Ni (II) and Cu (II) *bis*-(2-acetylthiophene) oxaloyldihydrazone complexes in Suzuki-Miyaura reaction of boronic acid with aryl halides in acetonitrile with good impacted catalytic activity of the product yields (from 62% to 82%).[19] The active catalyst complex as Ni(0) and Ni(I) intermediate compounds in Heck and Suzuki-Miyaura reaction resulted from one and/or two electron processes in the catalytic cycles, has been detected and studied recently.[20] In particular, air-stable Ni (II)- P^N^P triazine-phosphine cationic complexes initiated the C—C cross couplings.[21] Sun *et al*. reported the synergistic influence of Co (II) ion on Pd (II)/Co (II) catalyzed Suzuki-Miyaura cross coupling reaction in an aqueous media.[22] N^O-bidentate 2-(hydroxyimino)-1-phenylpropan-1-one coordinated to Co (II) ion in an octahedral geometry as an effective catalyst for Sonogashira Hagihara cross coupling of electron-rich and/or electron-poor substituted aryl halides of with alkyne derivatives.[23] Cobalt chloride catalyzed the cross coupling of 1,3-dienes (additives) within homogeneous complexation, as reported elsewhere.[24] Hu *et al*. developed Ni (II) *N*,*N*,*N*-tridentate pyrrolidine complexes as catalysts for the cross coupling reaction of secondary alkyl halides.[25] The high transmetalation of Co P^N^P-complexes as catalysts for Suzuki-Miyaura cross coupling reaction was discussed and reported recently through the attack of the nucleophile to the central metal of the catalyst.[26]

Carbon steel (C-steel) is a widely utilized construction material owing to its excellent mechanical characteristics and cheapness.[27–29] Unfortunately, it quickly undergoes corrosion through electrochemical and chemical reactions with the components of neighboring environment. Solutions of HCl are usually employed for industrial acid cleaning, pickling, oil well acidifying processes, and acid de-scaling. Due to the aggressiveness of the acid medium, C-steel corrodes roughly.[29] A corrosion inhibitor is predominantly added to aggressive acid media for diminishing the corrosion impact on metal surface during the previous processes. The chosen of convenient inhibitors fundamentally depends upon its concentration, type of acid, economic availability, temperature, environmental side effects, the occurrence of dissolved organic and/or inorganic species and the type of metallic material.[30] Organic compounds containing Schiff base groups >C=N—, S, P, O, N and aromatic rings are reported in literature as most efficient corrosion inhibitors for the metals and alloys in acidic solutions.[31] The chelates of Schiff bases form stable complexes neatly packed in the coordination metal ion sphere to generate another category of compounds for corrosion inhibition.[32–34]

Herein, air-stable and water soluble novel complex catalysts of Ni (II) and Co (II) ions with tetradentate *N*,*O*,*O*,*N*-salicyldiene thiadiazole ligand is mediated in the typical C—C and C—N cross coupling processes under sustainable conditions, homogeneously. Their catalytic potential is studied in different solvent systems. Furthermore, to the best of our knowledge, there is no obtainable research on the anticorrosive performance of such type of 5-di (sodium sulfonate salicylidene)-2,5-dihydrazinyl thiadiazole derivatives (i.e. H_2Sanp) and its Ni- and Co-pincer chelates in acidic solution. Hence, the present investigation reports the involving of H_2Sanp, Ni-Sanp and Co-Sanp as corrosion inhibitors for C-steel in 1.0 M HCl. The study is performed using electrochemical measurements (PDP and EIS) and complemented with the surface analysis (SEM/EDX).

2 | EXPERIMENTAL

2.1 | Materials and equipment

All reagents, which used in this work, are ordered from Merck and Acros. Particularly, they are applied without any treatment or purification. CHN-analyses were progressed using a GMBH VarioEl model V2.3 CHN apparatus. NMR spectroscopic scans were accomplished on a multinuclear FT-NMR spectrometer Bruker ARX400 within 400.1 MHz for the nucleus of hydrogen and 100.6 MHz for nucleus of carbon at ambient temperature. The ^{1}H and ^{13}C spectral signal shifts are presented in ppm. J_{HH} refers to coupling constants values between H nuclei in the spectral scans. Infrared spectroscopy (mixed with KBr as discs) are measured with Shimadzu FTIR-8101 Fourier Transform Infrared spectrophotometer in the range of wave number from 4000 to 400 cm^{-1}.

Ultraviolet–Visible spectroscopy was displayed within 1.0 cm quartz cells in a holder, which temperature controlled by connection to a water thermostatted bath. UV–Vis. spectra carried out using a Jasco UV–Vis spectrophotometer (model V-570) of wavelength from 200 to 900 nm. Conductivity magnitudes of the studied compounds were estimated by a Jenway conductivity meter model 4320 connected with an epoxy bodied conductivity cell (two electrodes, shiny). The calibration of the cell constant was carried out from 0.01 to 19.99 at room temperature. Magnetic susceptibility of Ni-Sanp and Co-Sanp were evaluated using a Gouy's balance, the diamagnetic correction was controlled by Pascal's contents and $Hg[Co(SCN)_4]$ as a calibrant. EIS-mass spectra were carried by using Waters API Quatroo Micro Triple Quadrupole electrospray ionization mass spectrophotometer in the both modes of positive and negative. All given chemical processes were carried out with a magnetic stirring and held at the given temperature in a controlled thermostated oil bath.

The C-steel composition which applied for the corrosion processes, is composed of (wt%) S, 0.04%; C, 0.15%; Mn, 0.70%; Si, 0.19%; Cr, 0.011%; Ni, 0.011%; the remaining is Fe. HCl (Merck 37%) was prepared as 1.0 mol dm^{-3} in the aqueous media (deionized water). H_2Sanp and its metal-pincers, Ni-Sanp and Co-Sanp were prepared with different from 50 to 250 mg L^{-1} in bidistilled water.

2.2 | Synthesis of 5-di (sodium sulfonate salicylidene)-2,5-dihydrazinyl thiadiazole, H_2Sanp

0.73 g (5.0 mmol) of 2,5-dihydrazinyl thiadiazole, which dissolved in 20 ml of EtOH, added to an aqueous solution of 2.24 g 5-sodium sulfonate salicylaldehyde (10.0 mmol, 30 ml) dropwisely. The mixed solution was refluxed for 2 hrs with stirred and reaction controlling by TLC to give yellow color solution. The binary mixed solvents were evaporated and the ligand was acquired in pure form by recrystallization in water-ethanol mixture (1: 1).

^{1}H NMR (DMSO-d_6, 400 MHz): δ 6.97 (d, $^3J = 7.7$ Hz, 2 H), 7.75 (dd, $^4J = 1.1$ Hz, $^3J = 7.5$ Hz, 2 H), 7.94 (d, $^4J = 1.2$ Hz, 2 H), 10.62 (s br, 2 H, CH=N) and 13.77 ppm (br s, NH, 2 H).

^{13}C NMR (100 MHz, DMSO-d_6, dept-135): δ 117.69 (CH), 119.96 (C_q), 122.72 (C_q), 130.28 (CH), 136.78 (C_q), 140.88 (C_q), 161.12 (C_q) and 192.82 ppm (CH, CH=N). (^{1}HNMR, ^{13}CNMR and dept-135 supported by Figures S1-S3, supplied in the supplementary materials).

2.3 | Preparation of metal complexes (co-Sanp and Ni-Sanp)

In an aqueous solution (40 ml) of H_2Sanp (2.78 g, 5.0 mmol) was poured slowly to an aqueous media (30 ml) of metal ion of $CoCl_2.6H_2O$ or $Ni(OOCCH_3)_2.4H_2O$ (1.24 or 1.18 g, 5.0 mmol), respectively. The mixed solution was heated for 3 hrs at 70 °C with continuous stirring. Color of the reaction media was turn into the given color of the novel complex. Water was removed by evaporation and the residual was recrystallized in water-ethanol binary mixture (1: 1) to give pure crystalline complex which dried in oven.

2.4 | Catalytic studies

Homogeneous cross coupling of Suzuki-Miyaura and Buchwald-hartwig reactions were performed in three necked round flask with water circulated condenser containing phenylboronic acid (1.0 mmol) or aryl amine (mesityl amine or 3-chloro aniline, 1.0 mmol) in 10 ml of the given solvent in presence of the complex catalyst (Ni-Sanp or Co-Sanp, 0.20 mmol) and potassium carbonate, as a base (2.0 mmol). The reaction was initiated by addition of aryl halide (bromobenzene or chlorobenzene, 1.1 mmol) under reflux conditions at 100 °C for 10 hrs. All catalytic reactions were carried out contacting to air in Schlenk system with magnetic stirring in a thermostated oil bath at the chosen reaction temperature.

The C—C or C—N cross coupling products were extracted by adding ethyl acetate as an organic layer. In the organic layer, water was removed by anhydrous $MgSO_4$ and then filtrated out. The products percentages were estimated and determined after reaction completion by injection to Shimadzu Gas Chromatography mass spectrometer (GC–MS) model QP2010 SE, which equipped with Rxi-5 Sil MS capillary column (30 m length × 0.25 mm ID × 025 um film thickness) at room temperature. The GC-Mass oven temperature was initiated to 40 °C and held for 1 min. The temperature rate was enhanced with 10 °C min^{-1} up to 200 °C. Operation of the inlet was carried out in the mode of split less at 200 °C was the mass spectra temperature of transfer line. The carrier gas was Helium with high purity up to 99.999%, which applied under rate of flowing 1 ml/min. Lab solution software, was applied to analyze the percentages yields of the obtained products.

2.5 | Corrosion inhibition measurements

The electrochemical investigations were completed in a traditional three-electrode cell consisting of C-steel specimen as working electrode, a platinum sheet as counter electrode and a saturated calomel electrode (SCE) as reference, using Versa STAT4 potentiostat/galvanostat (Princeton Applied Research, USA) at 30 °C. Electrochemical impedance spectroscopy (EIS) were completed utilizing AC signals of amplitude 10 mV peak-to-peak at the open circuit potential (E_{ocp}) after 60 min of immersion in the frequency domain of 10 kHz–0.1 Hz. The empirical EIS results were fitted to convenient equivalent circuit using ZView Software.

Potentiodynamic polarization (PDP) measurements were carried out at a sweep rate of 0.2 mVs^{-1} in the potential range ± 250 mV vs. SCE at E_{ocp}.

2.6 | Surface morphology by scanning electron microscopic (SEM) and energy dispersive X-ray spectroscopy analysis (EDX)

For surface analysis investigations of C-steel specimens in the blank and inhibited solutions, SEM and EDX spectra were applied using JEOL SEM, model-5300 attached with EDX unit with an 3.0 kV operating voltage.

3 | RESULTS AND DISCUSSION

3.1 | Synthesis and characterization

Newly, the condensation of 2,5-dihydrazinyl thiadiazole with 5-sodium sulfonate salicylaldehyde carried out sustainably, whereas the reaction with salicylaldehyde is already reported previously.[31] 2,5-Dihydrazinyl thiadiazole was prepared according to the published method previously,[2] which reacted with 5-sodium sulfonate salicylaldehyde in 1: 2 molar ratios, respectively, to afford H_2Sanp (Scheme 1).

Elemental analysis, NMR, UV–Vis., IR and mass spectroscopies were used to characterize the synthesized ligand. H_2Sanp coordinated to Ni^{2+} and Co^{2+} ions, as nickel acetate tetrahydrate and cobalt chloride hexahydrate, in an aqueous media to give Ni-Sanp and Co-Sanp, respectively, which synthesized in 1: 1 molar ratios of H_2Sanp to M^{2+} ion (Scheme 2). Ni-Sanp and Co-Sanp were characterized by IR, UV–Vis. and mass spectra, EA, TGA, conductivity measurements and magnetic susceptibility (Tables 1 and 2). Unfortunately, all attempts to grow single crystals of the metal complexes were failed for X-ray analysis (Figure 1).

The novel chelating ligand and its M-complexes are remarkable stable in the pH ranges from 1.6–9.7 using the standard universal buffer solutions.[34] Furthermore, H_2Sanp is soluble in water and little soluble in methanol, ethanol, acetone and acetonitrile, also, Ni-Sanp and Co-Sanp are soluble in water and slightly soluble in methanol, ethanol and acetonitrile. All compounds are not soluble in less or non-polar solvent, e.g. dichloromethane, carbon tetrachloride and toluene.

The elemental analyses of H_2Sanp, Ni-Sanp and Co-Sanp were investigated and listed in Table 1, which are in agreement with their suggested chemical formulas with little difference between the theoretical and the measured values is about ±0.4%.

In particular, the ^{1}H, ^{13}C NMR spectrum and dept-135 of H_2Sanp were measured in DMSO-d_6 at 25 °C and listed in Table 2, with supported supplementary materials in Figures S1-S3. The function protons of H_2Sanp could be estimated as a broad singlet signal at 13.77 ppm, which corresponded to the NH— group. Additionally, the proton of the azomethine group manifested a singlet sharp signal at 10.62 ppm. The rest signals are belonged to the aromatic ring. The characteristic spectral signals of ^{13}C NMR is 192 ppm for the carbon of azomethine group. On the other hand, Ni-Sanp and Co-Sanp are para-magnetic complexes in the suggested square planar and octahedral spherical structures with values 3.94 and 5.12 B.M., respectively, as reported magnetic values in Table 2.

Electronic spectrum of H_2Sanp and its corresponding pincer complexes (Ni-Sanp and Co-Sanp) deduces the characteristic absorption wavelength, λ_{max} (nm) and the derived molar absorptivity values, ε (mol^{-1} cm^{-1}) in and water, as depicted in Figure 2 and reported in Table 1. The UV-spectra for H_2Sanp assigned three bands at 226, 250 and 301 nm are attributable for to the intra ligand spin-allowed transitions $\pi \rightarrow \pi^*$, $\pi \rightarrow \pi^*$ and $n \rightarrow \pi^*$, respectively.[35] An additional band in the Visible-zone appeared at 338 nm, which is due to ligand charge transfer. All given bands of the ligand has been influenced by its complexation to Ni^{2+} or Co^{2+} ions, in which the three UV-bands were shifted to be 229, 244 and 295 nm for Ni-Sanp, and 224, 248 and 302 nm for Co-Sanp, respectively. Furthermore, the visible band for H_2Sanp was shifted also at 332 and 323 nm for Ni-Sanp and Co-Sanp, respectively.

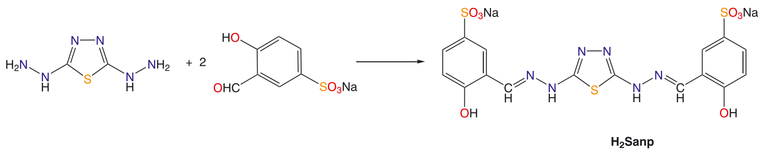

SCHEME 1 Synthetic route of 5-di (sodium sulfonate salicylidene)-2,5-dihydrazinyl thiadiazole (H_2Sanp)

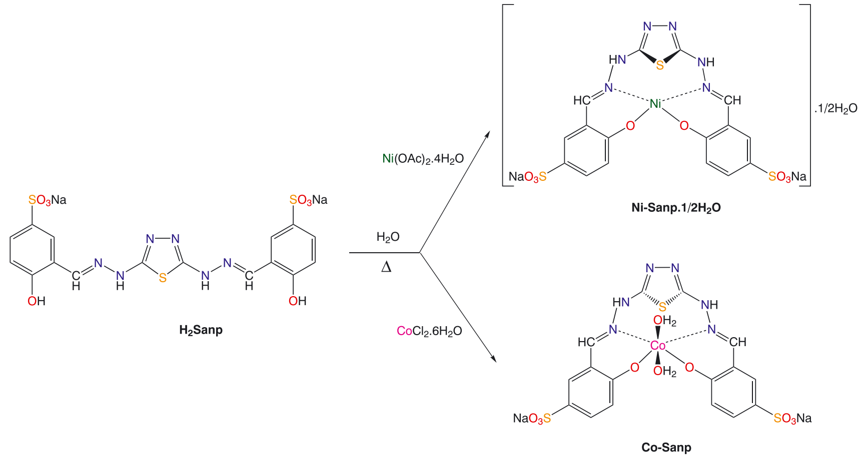

SCHEME 2 Complexation of H_2Sanp with Co^{2+} and Ni^{2+} ions

TABLE 1 Elemental analyses, yield, appearance, melting point in Celsius and UV–Vis. spectrum of H_2Sanp, Ni-Sanp and Co-Sanp at [compound] = 1.0 × 10^{-4} mol dm^{-3} in H_2O at room temperature, molar conductivity measurements (Λ_m) at [compound] = 1.0 × 10^{-3} mol dm^{-3} in dimethyl sulfoxide (DMSO) and *N*,*N*-dimethylformamide (DMF) at 25 °C

			CHN analysis found %, (calc. %)				Λ_m (Ω^{-1} cm^2 mol^{-1})			UV–Vis. spectra		
Compound	**MW (g mol^{-1})**	**Yield (%)**	**C**	**H**	**N**	**m.p. (°C)**	**DMSO**	**DMF**	**Color**	**λ_{max} (nm)**	**ε (mol^{-1} cm^{-1})**	**Assign.**
H_2Sanp	573.51	71	34.02 (34.41)	2.45 (2.17)	14.83 (15.05)	257	189	218	Yellow	338	10189	CT
										301	8604	n → π*
										250	12509	π → π*
										226	32811	π → π*
Ni-Sanp.1/2H_2O	615.15	84	30.22 (30.79)	1.95 (1.78)	13.77 (13.46)	> 300	211	236	Brown	371 br	7614	LM-CT
										332	9108	CT
										295	9312	n → π*
										244	26709	π → π*
										229	34921	π → π*
Co-Sanp	651.42	78	29.84 (29.50)	2.43 (2.17)	13.10 (12.90)	> 300	223	254	Green	425 v br	1187	LM-CT
										323	8233	CT
										302	9101	n → π*
										248	20093	π → π*
										224	45117	π → π*

vbr = very broad band

Additionally, a new broad band was observed at 371 and 425 nm for Ni-Sanp and Co-Sanp, respectively, which referring to LMCT (ligand to metal charge transfer), Figure 2.

The significant IR analysis of H_2Sanp and its Ni- and Co-complexes are listed in Table 2 and supported by Figures S9-S14 (supplied in the supplementary materials). The –OH phenolic vibrational broad band of H_2Sanp was detected at 3516 cm^{-1}, which disappeared within complexation to Ni^{2+} and Co^{2+} ions.[36] Such disappearing of the –OH band could be resulted from its coordination ability by deprotonation *via* oxygen to the metal ion. Remarked shifts of the characteristic vibrational $\bar{\nu}_{(\text{azo-methine})}$ of H_2Sanp from 1655 and 1621 cm^{-1} to 1619 and 1579 cm^{-1} for Ni-Sanp and to 1626 and 1601 cm^{-1} for Co-Sanp, respectively. Those shifts could be also resulted from the coordination binding of the nitrogen atom of the azo-methine group to Ni^{2+} and Co^{2+} ions. The number of coordinated water molecules in Co-Sanp could be remarked by a very broad band at 3424 cm^{-1}, which is different in value from the crystalline water molecules in Ni-Sanp (3338 cm^{-1}). That difference in stretching vibrational values between the crystalline and coordinated water molecules has been recorded recently[36,37] (Scheme 2). The significant vibrational band of the –NH has been

TABLE 2 Distinguished infrared spectra (ν^{-}, cm^{-1}) and magnetic susceptibility for H2Sanp and its Ni- and Co-complexes at 25 °C

Compound			
Group	**H_2Sanp**	**Ni-Sanp**	**Co-Sanp**
O—$H_{(water)}$	--	3338 w br	3424 w br
O—$H_{(phenolic)}$	3516 br w	--	--
N—H	3422 br m	3178 w br	3166 w br
C—H_{ar}	3069 m	--	--
C—$O_{(phenolic)}$		1216 w	1215 m
C=$N_{(azomethine)}$	1655 w 1621 m	1619 m 1579 w	1626 m 1601 m
C—N	1169 s 1103 s	1162 m 1100 s	1175 s 1104 s
C—S	1030 s	1031 s	1033 s
S—O^{-}	1474 m	1472 m	1469 m
S=O	1283 s	1286 w	1286 w
M—O	--	665 m	668 m
M—N	--	588 s	593 s
Magnetism (B.M.)	--	3.94	5.12

br = broad band, s = strong band, m = moderate band, w = weak band, ar = aromatic ring, al = aliphatic chain

intense influenced by the complexation of the azomethine group to the metal ion by shifting from 3422 to 3178 cm^{-1} and 3166 cm^{-1} in Ni-Sanp and Co-Sanp, respectively, as weak broad absorption bands. The stretching absorption bands of the S—O^{-} and S=O bonds of the sodium sulfonate group in H_2Sanp is detected at 1474 and 1283 cm^{-1}, respectively, which have not been influenced by the presence of metal ion. In Ni-Sanp, they appeared at 1472 and 1286 cm^{-1} and in Co-Sanp at 1469 and 1286 cm^{-1}.[34,38] Furthermore, new weak to medium absorption bands have been reported at 665 and 668 cm^{-1} for the new coordination bonding M—O and also at 588 and 593 cm^{-1} for the M—N bonding in Ni-Sanp and Co-Sanp, respectively (Table 2).[34,39] The stoichiometric ratios of metal ion to ligand were accomplished by applying of the spectrophotometric continuous variation method.[40] According to the continuous variation plot (Figure S10), it could be estimated that the Ni^{2+} or Co^{2+} ion coordinated to H_2Sanp in 1: 1 molar ratios.

Mass spectral measurements of H_2Sanp and its M-complexes were investigated to confirm their molecular structure as anion in the absence of Na^{+} ion in water/methanol solution (supported by Figures S7-S9 in

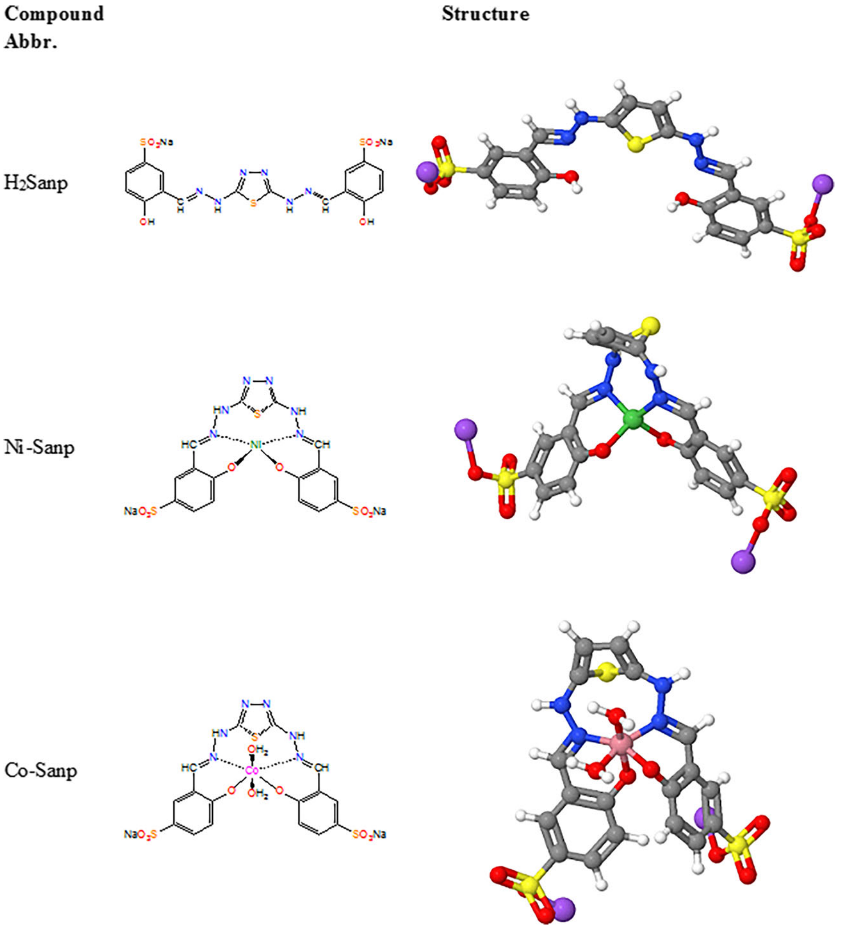

FIGURE 1 The tentative molecular structure of H_2Sanp, Ni-Sanp and Co-Sanp

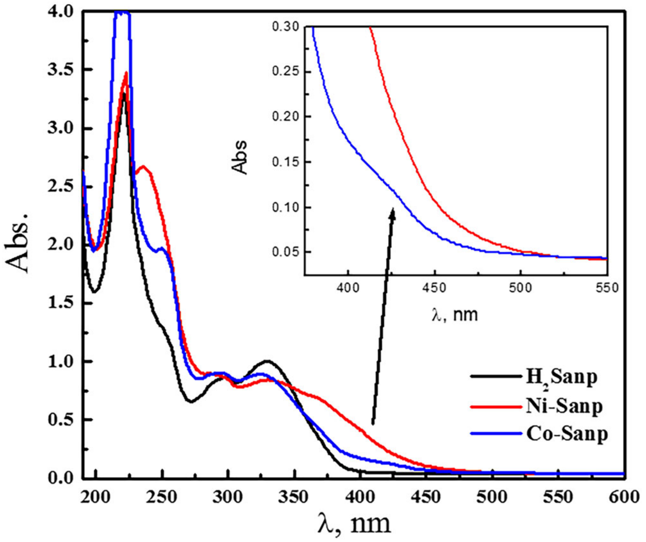

FIGURE 2 Electronic spectral scans of H_2Sanp, Ni-Sanp and Co-Sanp at [compound] = 1.0×10^{-4} mol dm^{-3} in H_2O at room temperature

the supplementary materials). An observable sharp signal in the negative mode for M-pincer complexes [M—Na$^+$ +1] appeared at 514 and 513 m/z for H_2Sanp, 570 and 606 m/z for Ni-Sanp and Co-Sanp, respectively. An additional peak of the loss of the two labile coordinated water molecules in Co-Sanp was detected at 570 m/z. In the positive mode, another peak with the loss of sulfonate group [M—SO_3^- + 1] displayed at 353 m/z for H_2Sanp and 410.0 and 410.2 m/z for both Ni-Sanp and Co-Sanp, respectively, as reported elsewhere for the sodium sulfonate Schiff base complexes.[38]

The crystalline and/or coordinated solvent species in the M-Sanp, i.e. water, could confirm by thermogravimetric analyses.[37] TGA results confirm the diagnostic number of water molecules in the crystal lattice in Ni-Sanp and Co-Sanp. Figure S11 (in the supplementary materials) demonstrated that Ni-Sanp contains a half water molecule for each Ni-complex molecule in the lattice, whereas, Co-Sanp does not have any water molecules in the crystal lattice. An observable decomposed successive step from 100 to 130 °C from Ni-Sanp mass was detected with Δm_{rel} = 1.6%, which are acceptable with the calculated mass loss ($\Delta \mathrm{m}_{\mathrm{rel}}$ = 1.4%). Particularly, Co-Sanp has a remarkable mass loss of two water molecules in the range from 170 to 230 °C in the thermogram 5.8% (Figure S11), which assigned for the two coordinated water molecules in Co-Sanp and agreed with the calculated mass loss (5.5%).[35] Considerably, Co-Sanp has an octahedral geometry, which coordinated to H_2Sanp within four-coordination bonding and completed within two labile coordinated water molecules (Scheme 2). Ni-Sanp could be considered as square planar complex.

From the molar conductivity measurements (Λ_m) of H_2Sanp, Ni-Sanp and Co-Sanp in DMSO and DMF, that all compounds are highly polar and consisting of four ions in the solution at 25 °C (Table 1). The high polarity of the studied compound is resulted from the attached *p*-sodium sulfonate group, which awards two counter ions in the given solvent, particularly of —SO_3^- and two cations of Na$^+$ ions.[7] From all possible characterization data, Scheme 2 presents the coordination chemical behavior of H_2Sanp towards Ni^{2+} and Co^{2+} ions, in which H_2Sanp acts as tetradentate dibasic pincer chelate. H_2Sanp coordinated to Ni^{2+} or Co^{2+} ion within the two nitrogen azo-methine groups and the two oxygen atoms of the deprotonated hydroxylphenyl groups. Finally, there is no detected action in the coordination behavior of the sulfur atom of the thiadiazole ring toward the metal ion. All attempts to crystalline the studied complexes and analyze them by X-ray crystallographic analyses were failed in various conditions.

3.2 | Catalytic studies

3.2.1 | Catalytic efficiency

The catalytic efficiency of the novel prepared Ni- and Co-*O*,*N*,*N*,*O*-complexes (Ni-Sanp and Co-Sanp) was devoted to the Suzuki C—C coupling of phenylboronic acid with 2-halopyridine (2-bromopyridine and 2-chloropyridine) and Buchwald-Hartewig C—N coupling of aryl amine (mesityl amine and 3-choroaniline) with 2-halopyridine (2-bromopyridine and 2-chloropyridine) in presence of excess amount of base, K_2CO_3. The catalytic system carried out in ethanol, water or ethanol-aqueous binary mixture to meet the sustainable conditions at 100 °C. To optimize the catalytic reaction conditions (time in hours) all catalytic processes were monitored by TLC and GC–MS. The reaction product yields at the optimal conditions of both C—C and C—N couplings are listed in Tables 3 and 4, respectively. The choice of K_2CO_3 as the base for the current catalytic system is due to the well combination of the catalyst with water, *i.e.* the solvent, and the base.[41] Initially, the C—N product yields were better than that of C—C product, which could be resulted from the less stability of boronic acid towards air and water compared to aryl amine as a substrate.[42]

In addition, the catalytic C—C and C—N reactions consumed less time with 2-bromopyridine than that with 2-chloropyridine for the optimized product yield percentages under all different various sustainable conditions.

TABLE 3 The Suzuki cross coupling reaction of phenylbronic acid with aryl halide catalyzed by either Ni-Sanp or Co-Sanp under various conditions

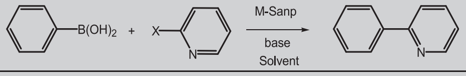

Entry[a]	Phenylbronic acid	Aryl halide	Catalyst	Solvent	Time, h	Yield (%)[b]
1	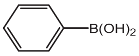	Bromopyridine	Ni-Sanp	H_2O	10	64
2		Chloropyridine	Ni-Sanp	H_2O	12	55
3		Bromopyridine	Co-Sanp	H_2O	11	60
4		Chloropyridine	Co-Sanp	H_2O	14	57
5		Bromopyridine	Ni-Sanp	EtOH:H_2O (1:1)	8	79
6		Chloropyridine	Ni-Sanp	EtOH:H_2O (1:1)	9	71
7		Bromopyridine	Co-Sanp	EtOH:H_2O (1:1)	7	75
8		Chloropyridine	Co-Sanp	EtOH:H_2O (1:1)	9	70
9		Bromopyridine	Ni-Sanp	EtOH	6	83
10		Chloropyridine	Ni-Sanp	EtOH	7	73
11		Bromopyridine	Co-Sanp	EtOH	6	80
12		Chloropyridine	Co-Sanp	EtOH	8	68

[a] Phenylbronic acid (1.0 mmol), aryl halide (1.1 mmol), base (K_2CO_3, 2.0 mmol), solvent (10 ml) and catalyst (0.20 mmol) at 100 °C.

[b] The yield amount percentages of the C—C product.

TABLE 4 The Buchwald-Hartwig amination reaction of aryl amine with aryl halide catalyzed by either Ni-Sanp or Co-Sanp under various conditions

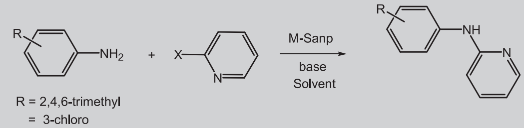

Entry[a]	Aryl mine	Aryl halide	Catalyst	Solvent	Time, h	Yield (%)[b]
1	Mesityl amine	Bromopyridine	Ni-Sanp	H_2O	8	80
2	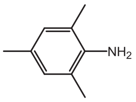	Chloropyridine	Ni-Sanp	H_2O	8	74
3		Bromopyridine	Co-Sanp	H_2O	10	83
4		Chloropyridine	Co-Sanp	H_2O	11	72
5		Bromopyridine	Ni-Sanp	EtOH:H_2O (1:1)	6	87
6		Chloropyridine	Ni-Sanp	EtOH:H_2O (1:1)	7	85
7		Bromopyridine	Co-Sanp	EtOH:H_2O (1:1)	8	89
8		Chloropyridine	Co-Sanp	EtOH:H_2O (1:1)	10	82
9		Bromopyridine	Ni-Sanp	EtOH	5	91
10		Chloropyridine	Ni-Sanp	EtOH	5	86
11		Bromopyridine	Co-Sanp	EtOH	5	92
12		Chloropyridine	Co-Sanp	EtOH	7	84
13	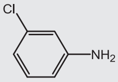	Bromopyridine	Ni-Sanp	H_2O	9	83
14		Chloropyridine	Ni-Sanp	H_2O	10	79
15		Bromopyridine	Co-Sanp	H_2O	7	88
16		Chloropyridine	Co-Sanp	H_2O	7	83
17		Bromopyridine	Ni-Sanp	EtOH:H_2O (1:1)	8	90
18		Chloropyridine	Ni-Sanp	EtOH:H_2O (1:1)	8	86
19		Bromopyridine	Co-Sanp	EtOH:H_2O (1:1)	9	91
20		Chloropyridine	Co-Sanp	EtOH:H_2O (1:1)	8	89
21		Bromopyridine	Ni-Sanp	EtOH	5	90
22		Chloropyridine	Ni-Sanp	EtOH	6	85
23		Bromopyridine	Co-Sanp	EtOH	7	88
24		Chloropyridine	Co-Sanp	EtOH	8	81

[a] Aryl mine (1.0 mmol), aryl halide (1.1 mmol), base (K_2CO_3, 2.0 mmol), solvent (10 ml) and catalyst (0.20 mmol) at 100 °C.

[b] The yield amount percentages of the C-N amination product.

The optimized yield of the chemoselective products of the C—C bonding formation of phenylboronic acid with 2-brmopyridine catalyzed by Ni-Sanp or Co-Sanp were obtained in ethanol with the less required time for the reaction completion (Table 3, entries 9–12) affording 83% with Ni-Sanp and 80% with Co-Sanp. With 2-chloropyridine, the resulted biaryl product was less than that with 2-brmopyridine in ethanol (entries 10 and 12, 73% for Ni-Sanp and 68% for Co-Sanp).

However, most of C—C and C—N coupling systems were achieved in organic solvents or in mixture of aqueous-organic solvent,[43] water is the most favored solvent for such catalytic systems under sustainable conditions but unsuitable solvent for the organic substrates due to the immiscibility and less solubility of the reaction mixture.[44] Particularly, the amount of the reaction products reduced from ethanol as the solvent, when water was presented in the reaction media (1: 1 of water: ethanol, entries 5–8), to pure water as the reaction solvent (e.g. for Ni-Sanp, 83% of the C—C product in ethanol, 79% in water-ethanol mixture and 64% in water, Table 3). Moreover, in the aqueous media, the C—C product was significantly consumed the longest time, smoothly (Table 3, entries 1–4). It is clear, that the solubility and miscibility of the reaction components could inhibit the catalytic potential of Ni-Sanp and Co-Sanp.[41,45] As aforementioned, the less stability of phenylboronic acid in the aqueous media diminished the C—C coupling products catalyzed by Ni-Sanp and Co-Sanp.

Similarly, the optimized solvent for the C—N cross coupling system was ethanol for the C—C coupling of mesityl amine with either 2-bromopyridine or 2-chloropyridine (Table 4, entries 9–12). Whereas, both ethanol and in the aqueous water-ethanol binary mixture are the optimized solvents for C—N coupling of 3-chloroaniline with 2-bromopyridine or 2-chloropyridine (entries 17–24). This is probably caused by the higher stability of aryl amines in water for the C—N coupling reactions.[46,47] Both C—C and C—N coupling reaction deigned respectable yields of the target products (as recorded in Table 3, entries1–4 and in Table 4, entries 1–4 and 13–17) with Ni-Sanp and Co-Sanp. Also, the Buchwald-Hartwig coupling reaction is more effective with M-Sanp than the Suzuki couplings.

The *p*-sodium sulfonate group could play a major role in the catalytic potential of the studied complexes by two entires, the first one is the type of internal base, *e.g.* K_2CO_3, K_3PO_4 or Na*t*BuO … .. within different cations. The second entry is the salt effect with various added salt to the catalytic processes with different cations, which probably have a remarkable influence.

3.2.2 | Mechanistic proposal and catalyst effect

Based on the reported typical mechanisms of C—C and C—N cross couplings,[23] the catalytic cycle started with formation of the active catalyst complex intermediate (**I**) by reduction of Ni^{2+} ion to Ni^0 in Ni-Sanp, and Co^{2+} ion to Co^0 in Co-Sanp within electron transfer.[18,26] Both phenyl boronic acid or aryl amine and the excess K_2CO_3 could be the reason for the reduction and formation of **I**.[48] An important step in the catalytic cycle could be proposed here due to the reaction of halopyridine, as an electrophile, with **I** to afford an octahedral geometrical addition of Ar^1—X accompanying oxidation of Ni^0 to Ni^{2+} or Co^0 to Co^{2+} giving the tentative intermediate (**II**), i.e. within oxidative addition, (Scheme 3). The oxidative addition of Ni-species has been elucidated by NMR by Manzoor *et al.*[20] and by Rull *et al.* of Ni-carbenes.[10] The excess amount of K_2CO_3 could raise the replacement of halide anion by the carbonate ion to give another intermediate (**III**). Due to the transmetalation,[26] the aryl group of the phenylboronic acid or the deprotonated aryl amine could bond to the metal ion with replacing of the carbonate group in the **III** in either Suzuki-Miyaura or Buchwald-Hartwig reactions, respectively, to produce an intermediate **VI**. Finally, the most significant step for reusing of the catalyst complex and formation of the chemoselective C—C or C—N product is the reductive elimination. In this step, the metal ion in **IV** reduced again to zero valet with forming of the active intermediate **I**. the liberated **I** is reused for another catalytic cycle.

The feasibility of the complex steric demand could be explored by the catalytic efficiency of the current complexes as catalysts for the C—C and C—N cross coupling processes.[49] The proposed square planar geometry of Ni-Sanp forced the reduction of Ni^{2+} ion and the substrate attack of halopyridine to the reduced Ni^0 ion in the oxidative addition step.[50–56] Moreover, the little more electronegativity of Ni^{2+} ion compared to that Co^{2+} ion could improve the Ni-Sanp catalytic potential due to the faster oxidative addition step achievement in the catalytic cycle more than that Co-Sanp.[23,57] The octahedral geometry of Co-Sanp could discourage its catalytic potentials. Therefore, it is clear here that why Ni-Sanp is little more effective catalyst for such reaction than Co-Sanp, which could also be emphasized by the yield of the C—C and C—N products under the optimal conditions (Tables 3 and 4). Despite the steric hindrance of the hard organic coordinated pincer ligand (H_2Sanp) and the little less electronegativity of Co^{2+} compared to Ni^{2+} in their complexes,[18] Co-Sanp has an appreciable catalytic activity. Besides, the little more electropositivity of Co^{2+} ion in Co-Sanp catalyst than that of

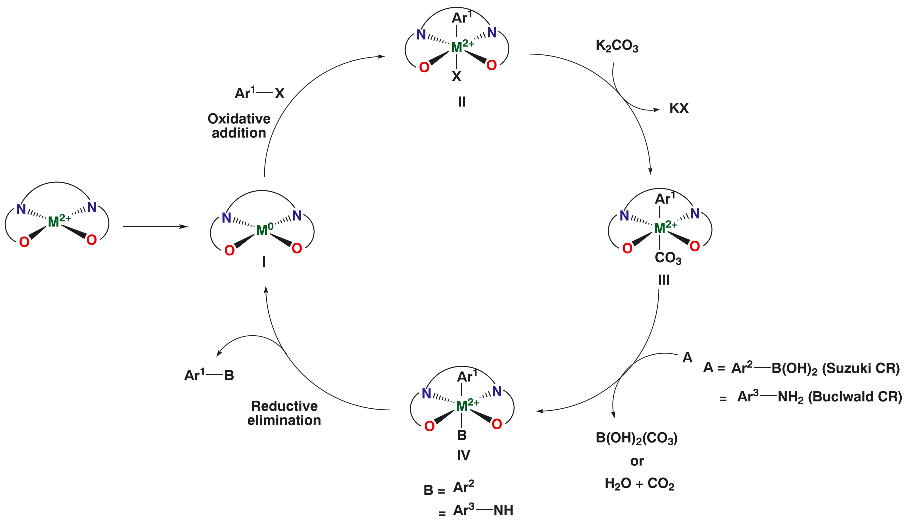

SCHEME 3 The mechanistic proposal of the Suzuki and Buclwald-Hartwig cross coupling reactions catalyzed by Ni-Sanp and Co-Sanp

Ni^{2+}-species could proceed the reductive elimination step in the catalytic cycle.[21,22,50–56]

By comparison our results of Ni-Sanp as square planar geometry to other reported octahedral Ni-*O*,*N*,*N*-benzoylhydrazone complex,[11,12] we explored that Ni-Sanp is more effective and sustainable catalyst for the Suzuki cross coupling reaction due to the steric effect. Moreover, the *cis*-structure of Ni-Sanp and Co-Sanp of the replaced group is the only possibility for the high catalytic potential of both Ni-Sanp and Co-Sanp. *Cis* form of both active catalysts intermediate (**IV**) of the two attached —Ar^1 and —B groups to the central metal ions could progress the reductive elimination step and improve the catalytic potential of Ni-Sanp and Co-Sanp. In the other hand, if the two functional groups in the intermediate (**IV**) are in *trans* position to each other, there will be no observable catalytic reactivity of the studied complexes and would give no chemoslelctive product of both C—C and C—N biaryl products.[58] Consequently, the reductive elimination step could proceed with

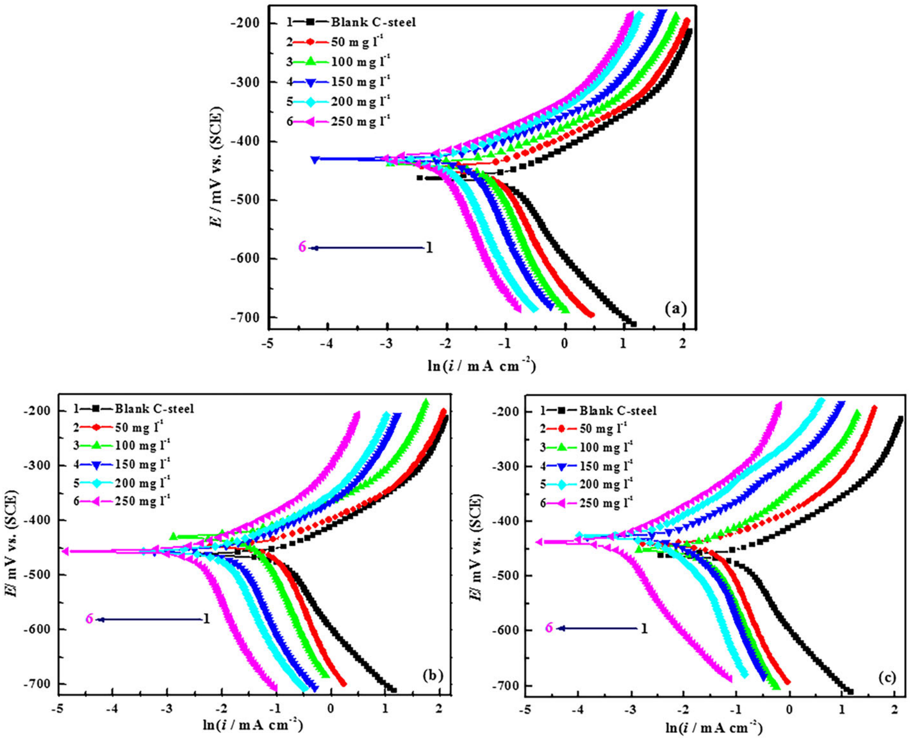

FIGURE 3 PDP behavior of C-steel in 1.0 N-HCl in the absence and presence of (a) H$_2$Sanp and its complexes, (b) Ni-Sanp and (c) Co-Sanp at 30 °C

retention of stereochemical structure of the homogeneous catalysts intermediate.[52–56]

3.3 | Corrosion inhibition performance

3.3.1 | PDP studies

In order to obtain information into the kinetics of metal dissolution processes and the hydrogen evolution reaction, PDP studies were carried out for C-steel in 1.0 M hydrochloric acid in the absence and presence of different doses of H_2Sanp and its Ni- and Co-complex inhibitors at 30 °C. Figure 3 shows the PDP plots for (a) H_2Sanp, (b) Ni-Sanp and (c) Co-Sanp, respectively. It could be inferred from the curves that the polarization plots style is conformable in both the inhibited and uninhibited medium. However, introducing of all inhibitors (H_2Sanp, Ni-Sanp and Co-Sanp) to the corrosive medium minimize the rate of C-steel corrosion as demonstrated in the shifting of the values of corrosion current density to lower regions in comparison to the uninhibited solution. Such result refers the corrosion inhibition capability of the investigated inhibitors. In addition, this phenomenon assigned that H_2Sanp, Ni-Sanp and Co-Sanp, suppressed both cathodic hydrogen evolution and steel anodic dissolution. It is also observed that the C-steel underwent active dissolution within the potential range investigated without propensity towards passivation in the free and inhibited solutions.

Table 5 records the related PDP illustrating the corrosion current density (i_{corr}), cathodic and anodic Tafel slope (β_c & β_a), corrosion potential (E_{corr}), and inhibition capacity (E_{PDP}), which were estimated from the polarization plots at 30 °C using extrapolation method.[59–61] From Table 5 and it corresponding plotting Figure 3, comparing to the free inhibitor solution, the E_{corr} value shifts mostly towards positive direction in the solution congaing inhibitors elucidating H_2Sanp, Ni-Sanp or Co-Sanp inhibitors, retards both the cathodic and anodic reactions. It is demonstrated that if the change in E_{corr} is more than 0.085 V verses E_{corr} of blank solution, affording the compound could be classified as a cathodic or an anodic type inhibitor. In case that the change in E_{corr} is lower than 0.085 V, the compound could be classified as a mixed type inhibitor.[62,63] Currently, the highest displacement in E_{corr} is about 37 mV, which is lower than 85 mV, suggesting that H_2Sanp and its complexes Ni-Sanp and Co-Sanp act as mixed type inhibitors. Moreover, i_{corr} value decreases dramatically in the presence of inhibitors, the value of i_{corr} for 250 ppm of Ni-Sanp or Co-Sanp is 57.45 or 35.63 μA cm^{-2}, respectively, much lower than that for H_2Sanp, *i.e.* 150.3 μA cm^{-2}. These data award that the inhibitive action of the Co- and Ni-complexes is better than that of H_2Sanp. The inhibition efficiency (E_{PDP}) and surface coverage (θ) are estimated according to the following equation[64]:

$$E_{PDP}(\%) = 100 \times \frac{i^o_{corr} - i^i_{corr}}{i^o_{corr}} = 100 \times \theta \qquad (1)$$

where i^o_{corr} and i^i_{corr} represent the corrosion current densities without and with the addition of inhibitors. From Table 5, there is no considerable change observed in the values of β_c & β_a by the inhibitor addition with respect to that blank solution, which indicate that addition of

TABLE 5 Corrosion parameters obtained from PDP for C-steel in 1.0 N-HCl in the absence and presence of the H_2Sanp and its Ni- and Co-complex inhibitors at 30 °C

Inhibitors code	C_{inh}/mg l^{-1}	i_{corr}/μAcm^{-2}	E_{corr}/mV (SCE)	β_a/mV dec $^{-1}$	-β_c/mV dec $^{-1}$	θ	E_{PDP}/%
Blank	0.0	1233	−464 ± 1%	78 ± 15%	137 ± 20%	-	-
H_2Sanp	50	504.05 ± 8%	−440 ± 2%	80 ± 10%	157 ± 5%	0.591	59.12
	100	430.68 ± 5%	−435 ± 2%	85 ± 14%	132 ± 6%	0.650	65.07
	150	277.54 ± 4%	−427 ± 4%	83 ± 8%	149 ± 11%	0.774	77.49
	200	198.01 ± 7%	−433 ± 1%	83 ± 18%	148 ± 13%	0.839	83.94
	250	150.30 ± 6%	−427 ± 3%	86 ± 12%	151 ± 15%	0.878	87.81
Ni-Sanp	50	398.50 ± 3%	−446 ± 1%	84 ± 14%	143 ± 17%	0.676	67.68
	100	296.41 ± 9%	−428 ± 2%	83 ± 10%	145 ± 14%	0.759	75.96
	150	153.50 ± 5%	−454 ± 2%	80 ± 19%	153 ± 16%	0.875	87.55
	200	90.25 ± 5%	−457 ± 4%	85 ± 17%	149 ± 7%	0.926	92.68
	250	57.45 ± 7%	−456 ± 2%	82 ± 10%	135 ± 8%	0.953	95.34
Co-Sanp	50	354.24 ± 4%	−438 ± 4%	81 ± 8%	140 ± 13%	0.712	71.27
	100	239.32 ± 7%	−450 ± 1%	83 ± 12%	142 ± 8%	0.805	80.59
	150	118.61 ± 5%	−427 ± 2%	79 ± 11%	144 ± 7%	0.903	90.38
	200	70.40 ± 6%	−422 ± 3%	81 ± 10%	149 ± 14%	0.942	94.29
	250	35.63 ± 6%	−438 ± 5%	83 ± 20%	139 ± 20%	0.971	97.11

H_2-Sanp and its complexes Ni-Sanp and Co-Sanp does not effect on the hydrogen reduction mechanism and the hydrogen evolution is activation-controlled.[65] Consequently, the adsorbed compounds act by unpretentious blocking of active sites for both cathodic and anodic reactions.[66] The E_{PDP} depends on different factors such as adsorption center, interaction mode, size and structure.[32] E_{PDP} increases with the compound doses. E_{PDP} of 250 ppm of H_2-Sanp, Ni-Sanp and Co-Sanp inhibitors reaches up to a maximum of 87.81%, 95.34% and 97.11%, respectively. This phenomenon may be explained by that the H_2-Sanp, Ni-Sanp and Co-Sanp molecules adsorbed on the surface of C-steel and forming a covering layer, which can act as a physical barrier to prevent diffusion of the corrosive species to the C-steel surface.

From Table 5, the higher E_{PDP} of Ni- and Co-complexes compared to H_2Sanp could be due to their big size and more active sites for adsorption. Such an increased activity of the Co- and Ni-pincer complexes may be interpreted based on of the theory of chelation.[67] On chelation, the metal ion polarity would be minimized to a greater extent because of the overlap of the H_2Sanp orbitals and partial sharing of the positive charge of the Co^{2+} and Ni^{2+} ions with donor groups. Co-Sanp displayed the highest E_{PDP} among the other compounds. Similar results were already reported for Co-complexes with Schiff base.[68] The sequence of E_{PDP} for the investigated inhibitors is Co-Sanp > Ni-Sanp > H_2Sanp. This order of E_{PDP} may also be interpreted in terms of the size of the central metal ion Co (II) > Ni (II).

3.3.2 | EIS studies

Figure 4a illustrates the Nyquist plots for the C-steel measured in the absence and presence of inhibitors (1-a) H_2Sanp, (2-a) Ni-Sanp and (3-a) Co-Sanp with different concentrations. Obviously, the Nyquist curves for the

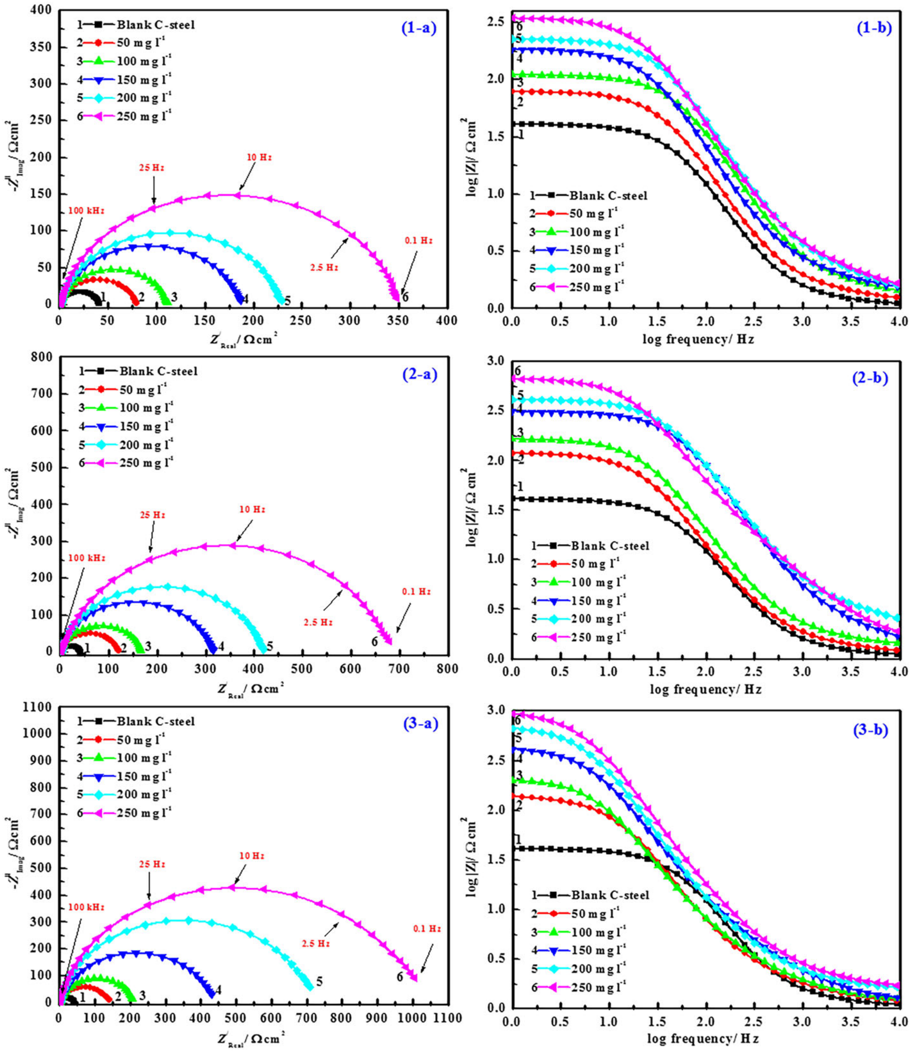

FIGURE 4 (a) Nyquist (b) Bode angle curves for C-steel in 1.0 N-HCl in the absence and presence of various dose of (1) H_2Sanp, (2) Ni-Sanp and (3) Co-Sanp at 30 °C

inhibited and uninhibited solutions are consisting of one depressed capacitive semicircle corresponding to one-time constant in the Bode curve (Figure 4b). The Nyquist plot shape is the same in the blank and inhibited solutions indicating no change in the mechanism of corrosion process. However, the diameter of the capacitive semicircle remarkably increased with the addition of inhibitors indicating that these compounds formed an effective layer on C-steel. Moreover, Nyquist curves display several inductive loops in the low frequency area, which is related to the relaxation adsorbed molecule of inhibitors on the surface of electrode.[69,70] The Bode modulus, Figure 4 (1-b, 2-b and 3-b), showed a single time constant, which agreed with the Nyquist plots. The absolute Bode modulus values are shifted to the higher values in the low frequency area with increment in the inhibitor doses. In another words, the corrosion inhibition could be performed by higher concentration of inhibitors than lower concentrations.

Comparison of empirical EIS results (points) measured for C-steel in blank 1.0 M HCl (1) and containing 250 mg L^{-1} of Ni-Sanp (2) inhibitor and the simulated data by Z-view software (line): (a) Nyquist plot and (b) bode phase modules are presented in Figure 5. Inset (Figure 5a) suggested equivalent electric circuit (EEC) utilized to fit the EIS data. This EEC consists of the constant phase element (CPE), the solution resistance (R_s) and the polarization resistance (R_p). In the current EEC analysis, the difference between the real impedance at higher and lower frequencies described as R_p rather than more usually applied resistance of charge transfer (R_{ct}). The standard behind using R_p is according to the fact that the C-steel corroding in acidic solution is mostly commitment to other kinds of resistances including film resistance (R_f), accumulation resistance (R_a), diffusion resistance (R_d) and along with R_{ct}, i.e. $R_p = R_{ct} + R_f + R_a + R_d$.[71–73] Some EIS parameters like R_s and R_p, double layer capacitance (C_{dl}) and phase shift (n) were derived using EEC and tabulated in Table 6. The inhibition efficiencies (E_{EIS}/%) at various studied concentrations have been calculated from the polarization resistances in the absence (R_P^0) and presence (R_P^i) of inhibitors by using Equation 2[38]:

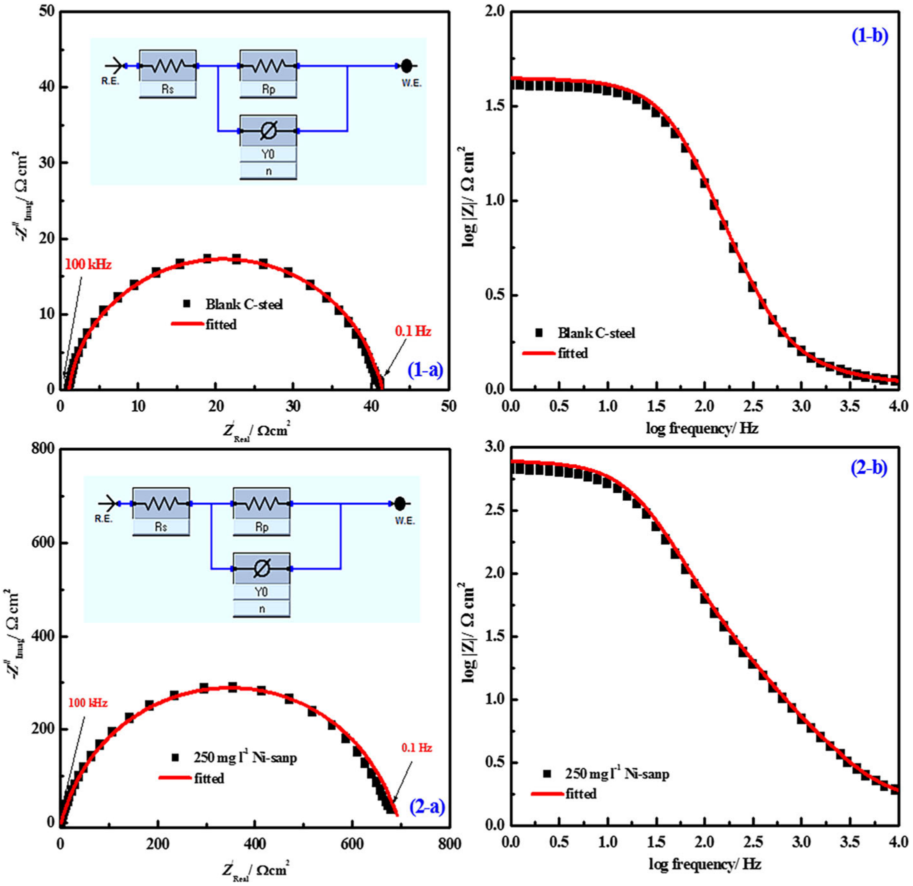

FIGURE 5 Comparison of empirical impedance results (points) measured for C-steel in blank 1.0 N-HCl (1) and containing 250 mg L^{-1} of Ni-Sanp inhibitor (2) and the simulated data (line): (a) Nyquist plot and (b) Bode phase modules. Inset (Figure 4-a) suggested equivalent electric circuit (EEC) utilized to fit the EIS data

TABLE 6 EIS parameters for C-steel and the inhibition efficiencies (E_{EIS}/ %) of different doses of the synthesized H_2Sanp and its Ni- and Co- complexes in 1.0 N-HCl at 30 °C

				Φ_{CPE}				
Inhibitors code	**C_{inh}/mg l^{-1}**	**R_s/Ω cm^2**	**R_p/Ω cm^2**	**Y_0/F cm^{-2} S^n × 10^{-6}**	***n***	**C_{dl}/F cm^{-2} × 10^{-6}**	**θ**	**E_{EIS}/ %**
Absence	0	1.05	42.7 ± 5%	136.2	0.776 ± 2%	95.10 ± 11%	-----	-----
H_2Sanp	50	1.10	81.6 ± 3%	78.5	0.887 ± 1%	50.2 ± 9%	0.476	47.6
	100	1.16	117.5 ± 8%	54.5	0.876 ± 4%	33.4 ± 12%	0.636	63.6
	150	1.21	197.8 ± 6%	36.8	0.902 ± 1%	24.6 ± 14%	0.784	78.4
	200	1.25	238.4 ± 7%	21.9	0.907 ± 3%	15.3 ± 10%	0.820	82.0
	250	1.32	368.8 ± 4%	10.8	0.917 ± 5%	7.3 ± 12%	0.884	88.4
Ni-Sanp	50	1.04	123.6 ± 9%	56.8	0.907 ± 4%	39.6 ± 10%	0.654	65.4
	100	1.12	170.1 ± 10%	39.3	0.897 ± 3%	26.3 ± 17%	0.748	74.8
	150	1.17	332.2 ± 8%	24.3	0.927 ± 2%	18.5 ± 16%	0.871	87.1
	200	1.80	443.4 ± 7%	16.3	0.929 ± 5%	12.4 ± 15%	0.903	90.3
	250	2.9	726.7 ± 9%	6.1	0.938 ± 6%	4.7 ± 11%	0.941	94.1
Co-Sanp	50	1.41	153.2 ± 6%	50.4	0.925 ± 5%	38.4 ± 8%	0.721	72.1
	100	1.52	220.1 ± 8%	31.1	0.917 ± 7%	22.6 ± 10%	0.806	80.5
	150	2.33	455.4 ± 5%	20.9	0.938 ± 8%	16.6 ± 11%	0.906	90.6
	200	1.76	751.8 ± 4%	12.7	0.948 ± 5%	10.5 ± 12%	0.943	94.3
	250	2.57	1088.5 ± 5%	4.2	0.949 ± 2%	3.3 ± 20%	0.961	96.1

$$E_{EIS}/\% = \left(1 - \frac{R_P^0}{R_P^i}\right) \times 100 = \theta \times 100 \tag{2}$$

Generally, for a metal/solution corroding system, CPE is being used instead of pure capacitor because of the presence of inhomogeneity surface. Impedance of the CPE (Z_{CPE}) could be exemplified by Equation 3[34]:

$$Z_{CPE} = \left(\frac{1}{Y_0}\right)[J\omega_n]^{-1} \tag{3}$$

where *j, n*, Y_0 and ω are imaginary number, phase shift, CPE constant and angular frequency, respectively. The lower value of *n* is associated with surface inhomogeneity and vice versa. It is observed to an increase in *n* values in the inhibited solutions compared to the blank (Table 6), indicating that surface morphology of in the presence of inhibitors have been smoothened uncommonly because of the adsorption of studied H_2Sanp and its Ni- and Co-complexes on the metal surface. Similar observation has been mentioned by our working group previously,[74] which was related to a decrease in heterogeneity resulting from the inhibitor molecules adsorption on the surface of C-steel. Moreover, to the surface inhomogeneity *n* value could be also applied for investigated the impedance spectra nature as value of $n = 1, 0.5, 0$ and -1 represent capacitance, Warburg impedance resistances and inductance and, respectively.[75] In current work, *n* values in the presence and absence of investigated H_2Sanp and its Ni- and Co- complexes change from 0.776 to 0.949 and are partially deviated from unity. This deviation type from ideal behavior is related to the inhomogeneity surface caused from interfacial and structural origin.[70] The values capacitance of double layer (C_{dl}) was calculated from the frequency at which the imaginary component of the impedance is extreme (ω_{max}) using the Equation 4[75]:

$$C_{dl} = Y_0[\omega_{max}]^{n-1} \tag{4}$$

where $\omega_{max} = 2\pi f_{max}$, f_{max} is the frequency at which the imaginary impedance component is maximum. The cautious inspection of data presented in Table 6 it displays that R_p value increased and C_{dl} values decreased in the inhibited solution predominantly at higher H_2Sanp and its Ni- and Co-complexes dose. These observations indicate that the studied ligand and its complexes adsorbed at the C-steel/HCl interfaces and subsequently increased electric double layer thickness and prevent acidic corrosion of C-steel.[76] Generally, the organic inhibitors have a larger volume than H_2O molecule and a much lower dielectric constant.[77] The lower values of C_{dl} in the inhibited media might be also related to the piecemeal replacement of H_2O molecules by the adsorption of the inhibitor species at steel surface. The protective film thickness is related to C_{dl} based on the Helmholtz model[78]:

$$\delta = \frac{\varepsilon\varepsilon_0 A}{C_{dl}} \tag{5}$$

where A, ε, ε_0 and δ are the geometrical electrode surface area, the medium dielectric constant, the vacuum permittivity and the protective film thickness, respectively. As the inhibitor dose increased, more molecules adsorbed onto the surface of C-steel, leading to a diminished immersion surface area of the electrode, lower local dielectric constant and an intensive electric double-layer. These observations caused reduce in C_{dl} values. Under a specific dose (250 mg L^{-1}), E_{EIS} of the three studied inhibitors calculated by Equation 2 obey the order of Co-Sanp > Ni-Sanp > H_2-Sanp, which is in a good consistent with the data of PDP. The maximum E_{EIS} is 96.1% in the presence of 250 mg L^{-1} Co-Sanp.

3.3.3 | Adsorption isotherm and corrosion inhibition mechanism

Adsorption of organic inhibitor species at the C-steel/solution interface consists of the modification of H_2O molecules by inhibitor species based on the following process (Equation 6)[79]:

$$Inhibitor_{sol} + zH_2O_{ads} \rightarrow Inhibitor_{ads} + zH_2O_{sol} \qquad (6)$$

where z is the number of H_2O molecules substituted by the inhibitor species, $\text{Inhibitor}_{(ads)}$ and $\text{Inhibitor}_{(sol)}$ are inhibitor species in the adsorbed on the steel surface and solution, respectively. Several adsorption isotherms including Freundlich, Bockris–Swinkels, Langmuir, Flory–Huggins and Temkin isotherms could be applied to fit the values of surface coverage (θ) at various concentrations in order to determine the adsorption behavior of the investigated inhibitors. Langmuir adsorption model is the preferable characterization of the adsorption behavior of the inhibitor species on the C-steel surface. Langmuir model was presented in Equation 7[80]:

$$\frac{C_{inh}}{\theta} = C_{inh} + \frac{1}{K_{ads}} \qquad (7)$$

where θ is the surface coverage, which is calculated from Equations 1 and 2; $C_{inh.}$ is the inhibitor dose and K_{ads} is the adsorption equilibrium constant (L mol^{-1}). Plot of $C_{inh.}/\theta$ versus $C_{inh.}$ yield a straight line and the slope is close to unity (Table 7). The value of R^2 (correlation coefficient) is more than 0.995 for all studied inhibitors (H_2Sanp, Ni-Sanp and Co-Sanp). Therefore, the model of Langmuir is suitable for the adsorption behavior of H_2Sanp, Ni-Sanp and Co-Sanp inhibitors on C-steel surface (Figure 6). Then, the values of K_{ads} are estimated from the straight lines intercepts, and the calculated values are listed in Table 7. The higher K_{ads} values indicate the higher coverage rate and therefore a best protective film of the compounds on the surface of C-steel.[81]

TABLE 7 Adsorption parameters for H_2Sanp and its Ni-, Co-complex inhibitors estimated from Langmuir adsorption model for C-steel in 1.0 N HCl at 30 °C

Inhibitors	Slope values	K_{ads} mol^{-1} L	Correlation coefficient (R^2)	ΔG^o_{ads} kJ mol^{-1}
H_2Sanp	0.992	12.6×10^4	0.995	−39.72
Ni-Sanp	1.010	18.8×10^4	0.998	−40.71
Co-Sanp	0.959	23.8×10^4	0.999	−41.33

By inspection Table 7, the K_{ads} value of Ni-Sanp and Co-Sanp complexes is greater than that of ligand, H_2Sanp, which is in agreement with the trend of the E_{EIS} and E_{PDP} calculated by EIS and PDP measurements. Moreover, the K_{ads} value is related to the standard free energy of adsorption process (ΔG^0_{ads}) by Equation 8[82]:

$$\Delta G^0_{ads} = -RTln(K_{ads} \times 55.50) \qquad (8)$$

where R and T represent the universal gas constant and the absolute temperature, respectively. The value of

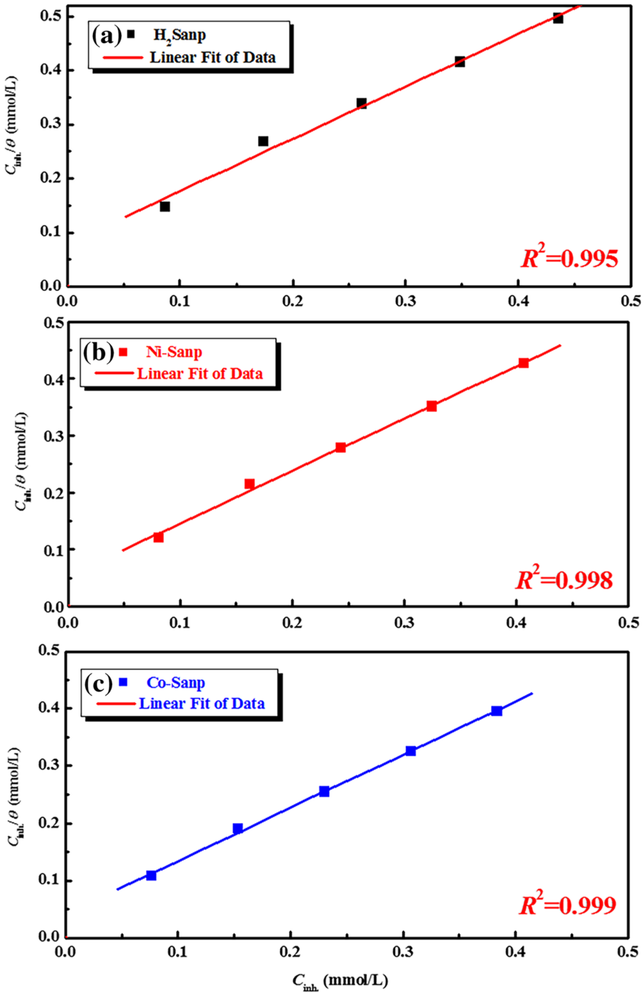

FIGURE 6 Langmuir adsorption model for (a) H_2Sanp, (b) Ni-Sanp and (c) Co-Sanp on the C-steel surface in 1.0 N-HCl at 30 °C

55.50 is the molar concentration of H_2O. Generally, the ΔG^0_{ads} values in the range of −20 to −40 kJ/ mol are consistent with the physical-adsorption.[83] While, higher ΔG^0_{ads}values than −40 kJ/ mol is dedicated to the chemical-adsorption.[84] According to the data in Table 7, the values of ΔG^0_{ads} for H_2Sanp, Ni-Sanp and Co-Sanp are −39.72, −40.71 and − 41.33 kJ/mol, respectively. Therefore, H_2Sanp, Ni-Sanp and Co-Sanp inhibitors are adsorbed onto the steel surface by mixed mechanism that involves chemical and physical adsorption.[85] In addition, the more negative ΔG^0_{ads} value of Co-Sanp and Ni-Sanp inhibitors represents a more stable adsorption film of Co-Sanp and Ni-Sanp molecules on the surface of metal in comparison with that of H_2Sanp.

The process of adsorption is affected by the inhibitor chemical structure, the charge of the steel surface and the charge of the inhibitor species. The potential of zero charge (E_{PZC}) of C-steel in 1.0 M HCl solution containing 250 ppm of H_2Sanp, Ni-Sanp and Co-Sanp inhibitors was estimated by using EIS method. The minimum on C_{dl} versus applied potential (E) plots (Figure 7) is considered as the E_{PZC} value of C-steel. The charge of metal surface can be determined by the position of E_{ocp} towards the E_{PZC}. The net C-steel charge at E_{ocp} was estimated based on Equation 9:

$$E_r = E_{ocp} - E_{PZC} \tag{9}$$

where E_r is the Antropov's corrosion potential.[85] The values of E_r at E_{ocp} values are +0.045, +0.041 and + 0.05 V for H_2Sanp, Ni-Sanp and Co-Sanp, respectively. This means that the C-steel surface in the inhibited solutions is positively charged at E_{ocp} in presence of 250 mg L^{-1} of H_2Sanp, Ni-Sanp and Co-Sanp. Therefore, Cl^- ions in aqueous solutions of HCl get adsorbed on the surface of C-steel. After the Cl^- ions adsorption, the C-steel surface becomes negatively charged. Subsequently, the protonated positively charged form H_2Sanp, Ni-Sanp and Co-Sanp inhibitors adsorbed on the C-steel surface by physical adsorption by electrostatic interactions with the Cl^- ions, which previously adsorbed on surface of metal.

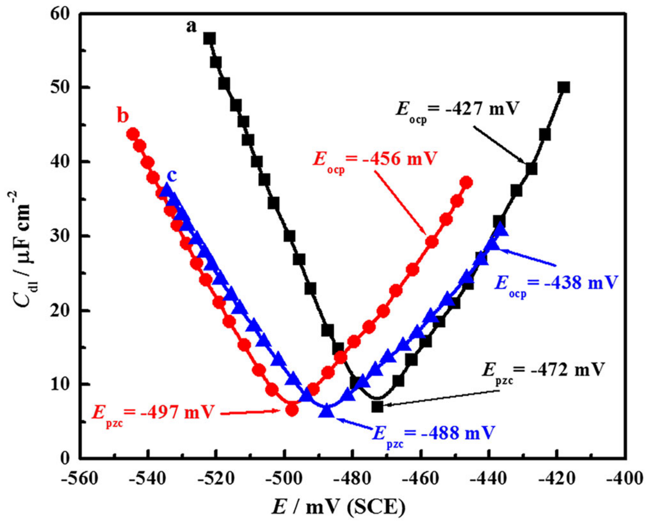

FIGURE 7 The plot of C_{dl} vs. applied potential for C-steel in 1.0 N-HCl solution containing 250 ppm of (a) H_2Sanp (black line), (b) Ni-Sanp (red line) and (c) Co-Sanp (blue line) at 303 K

In addition to physical adsorption, donor–acceptor interactions between the π-electrons of aromatic benzene ring and the unshared electron pairs of heteroatoms N and O with the vacant d-orbitals of Fe, this process is a chemical adsorption mechanism.[85] The schematic representation of the adsorption behavior of H_2Sanp on C-steel in 1.0 M HCl solution is shown in Figure 8. Therefore, the results approved that both chemical and physical adsorption together existed on the HCl/inhibitor/C-steel interface obtained from adsorption isotherm.

3.3.4 | Surface analysis by SEM and EDX

In order to recognize any changes occurred during process of corrosion in the absence and presence of studied ligand and its complexes, SEM analysis is carried out. SEM images of C-steel substrate exposure to blank 1.0 M HCl and in the inhibited solution containing 250 mg L^{-1} of Co-Sanp inhibitor for 48 hr are shown in Figure 9 (a-I and b-I). The C-steel morphology in the absence of inhibitor (blank HCl) (Figure 9 a-I) is very coarse and the surface is severely damaged because of dissolution of metal and contains some pores and cavities (represented by arrows). In contrast, the presence of 250 mg L^{-1} of Co-Sanp prohibits the corrosion rate and the surface damage has been minimized frequently (Figure 9 b-I) as compared to the uninhibited solution (Figure 9 a-I), indicating formation of a covering inhibitor layer at the surface of C-steel, which isolates the contact between the corrosive medium and the metal surface.

EDX analysis was performed to obtained knowledge about the composition of the C-steel surface in the blank and inhibited solutions. The EDX spectrums of C-steel after immersion in blank HCl and in the presence of 250 ppm of Co-Sanp for 48 hr are presented in Figures 9 (a-II and b-II). The EDX spectrum in blank solution shows peaks of Mn, C, Cr, Ni, Si, Fe, Cl, and O, indicating the formation of corrosion products (iron chloride and iron oxides) on the surface of C-steel. These observations indicate that the metal surface was strongly corroded in blank HCl. Whereas in the inhabited solution additional peaks for Na, N, S, and Co corresponding to the elements present in the Co-Sanp molecules, indicating the Co-Sanp molecules adsorption at the C-steel surface. Moreover,

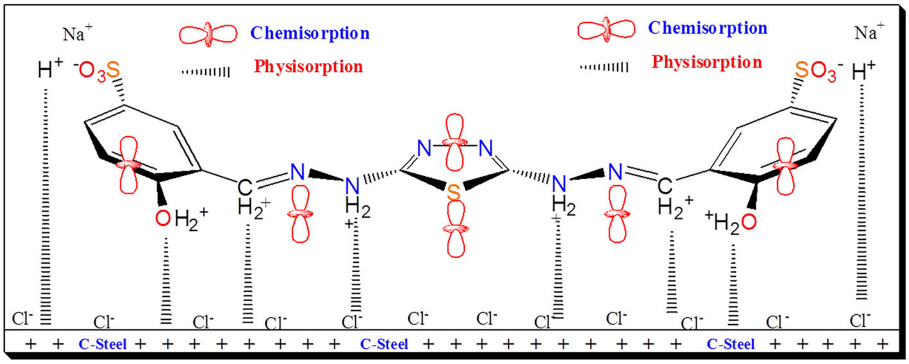

FIGURE 8 Schematic exemplification of the adsorption behavior of H_2Sanp on C-steel surface in 1.0 N-HCl solutions

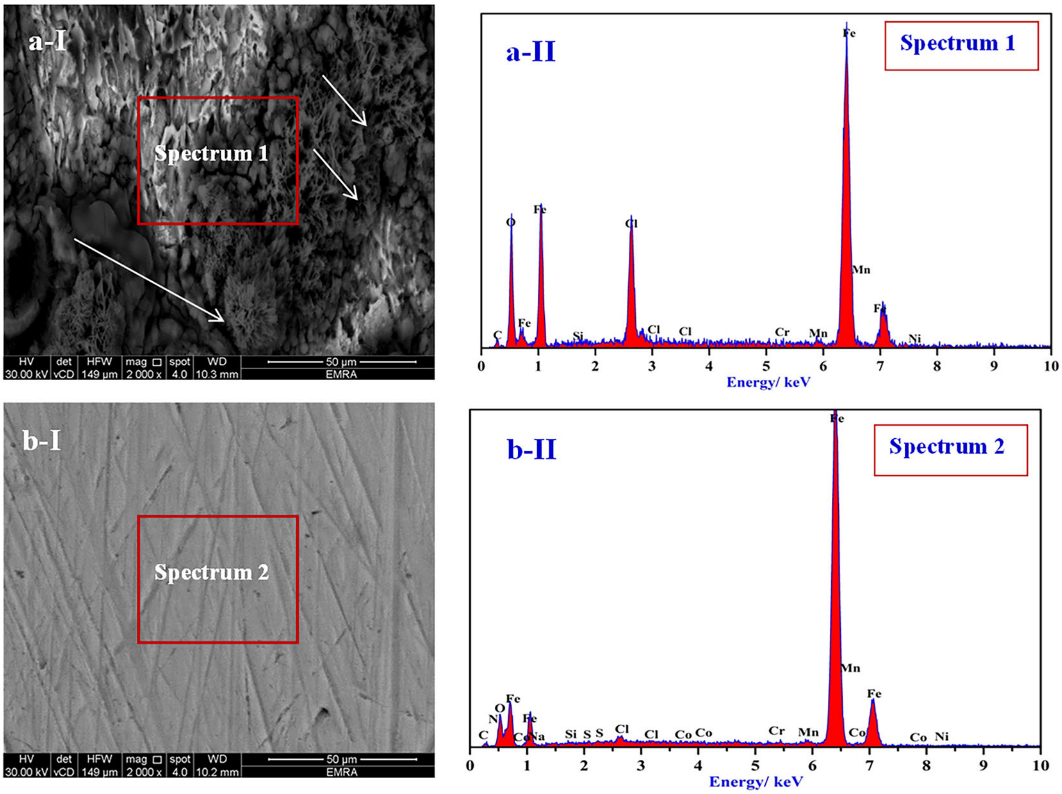

FIGURE 9 SEM pictures (I) and EDX spectra (II) of the C- steel surfaces after 48 hr exposure in 1.0 N-HCl solutions in the absence (a) and presence of 250 mg L^{-1} Co-Sanp (b) at 30 °C

the EDX spectra displays that there is a reduction in the corrosion products amount (iron chloride and iron oxides) where the peaks consistent with Cl and O formed because of the corrosion process are minimized. These results confirmed the inhibitory layer formed on the surface of C-steel.

4 | CONCLUSIONS

High stable and water soluble Ni- and Co-complexes (Ni-Sanp and Co-Sanp) were synthesized and characterized by complexeation to tetradentate pincer *N*,*O*,*O*,*N*-salicyldiene thiadiazole ligand (H_2Sanp). The catalytic efficiency of the two complexes was studied under sustainable conditions in the Suzuki C—C and Buchwald-Hartwig C—N cross coupling reactions. Both complexes afforded moderate to high catalytic potential towards C—C and C—N couplings, whereas Ni-Sanp showed higher catalytic reactivity. The steric hindrance of octahedral geometry of Co-Sanp compared to the square planar of Ni-Sanp and types of the central metal ion have distinguished effects on their potentials. The best solvent system for the C—C and C—N couplings is ethanol,

ethanol-water (1: 1) and then water under sustainable conditions, which could be due to the solubility and miscibility of the substrates in the catalytic processes.

EIS and PDP measurements have showed that the synthesized H_2Sano and its complexes Ni-Sanp and Co-Sanp are good inhibitors for the C-steel corrosion in acidic solution and the E_{EIS}/% and/or E_{PDP}/% increases with the inhibitor dose. The maximum inhibition capacity values obtained from PDP method for H_2Sanp, Ni-Sanp and Co-Sanp are 87.81%, 95.34% and 97.11% at 250 mg L^{-1}, respectively. The investigated H_2Sano and its complexes Ni-Sanp and Co-Sanp act as mixed-type corrosion inhibitors. Adsorption of compounds is characterized according to Langmuir model. Both chemical and physical adsorption phenomena are present but the chemisorption is predominant. Surface morphological analyses (SEM and EDX) emphasize the formation of adsorption layer of these inhibitors on the surface of C-steel.

ACKNOWLEDGMENTS

This work was supported by the grants from the Deanship of Scientific Research, King Faisal University (project number 180084). The financial contribution is gratefully acknowledged.

ORCID

Hany M. Abd El-Lateef https://orcid.org/0000-0002-6610-393X

Mohamed Shaker S. Adam https://orcid.org/0000-0001-8826-3558

REFERENCES

[1] P. J. Steel, *Adv. Heterocycl. Chem.* **1997**, *67*, 1.

[2] D. E. Jackman, *J. Heterocyclic Chem.* **1990**, *27*, 1053.

[3] A. R. Sayed, S. S. Al-Shihry, *Molecules* **2017**, *22*, 336.

[4] A. R. Sayed, *Turk. J. Chem.* **2015**, *39*, 600.

[5] M. Mastalir, E. Pittenauer, B. Stoger, G. Allmaier, K. Kirchner, *Org. Lett.* **2017**, *19*, 2178.

[6] J.-P. Corbet, G. Mignani, *Chem. Rev.* **2006**, *106*, 2651.

[7] A. M. F. Phillips, A. J. L. Pombeiro, *ChemCatChem* **2018**, *10*, 3354.

[8] A. De Meijere, F. Diederich, *Metal-Catalyzed Cross-Coupling Reactions*, 2nd ed., Wiley-VCH, Weinheim, Germany **2004**.

[9] N. Devi, K. Sarma, R. Rahaman, P. Barman, *Dalton Trans.* **2018**, *47*, 4583.

[10] S. G. Rull, I. Funes-Ardoiz, C. Maya, F. Maseras, M. R. Fructos, T. R. Belderrain, M. C. Nicasio, *ACS Catal.* **2018**, *8*, 3733.

[11] S. Gu, J. Du, J. Huang, Y. Guo, L. Yang, W. Xu, W. Chen, *Dalton Trans.* **2017**, *46*, 586.

[12] P. K. Suganthy, R. N. Prabhu, V. S. Sridevi, *Inorg. Chim. Acta* **2016**, *449*, 127.

[13] A. R. Hajipour, F. Rezaei, Z. Khorsandi, *Green Chem.* **2017**, *19*, 1353.

[14] R. Ghanbaripour, M. Samadizadeh, G. Honapisheh, M. Abdolmohammadi, *Synlett* **2015**, *26*, 2117.

[15] F.-S. Han, *Chem. Soc. Rev.* **2013**, *42*, 5270.

[16] M. Bagherzadeh, N. Mousavi, M. Zare, S. Jamali, A. Ellern, L. K. Woo, *Inorg. Chim. Acta* **2016**, *451*, 227.

[17] P. Saha, M. A. Ali, P. Ghosh, T. Punniyamurthy, *Org. Biomol. Chem.* **2010**, *8*, 5692.

[18] L. M. Kumar, B. R. Bhat, *J. Organomet. Chem.* **2017**, *827*, 41.

[19] D. P. Singh, D. S. Raghuvanshi, K. N. Singh, V. P. Singh, *J. Mol. Catal. A* **2013**, *379*, 21.

[20] A. Manzoor, P. Wienefeld, M. C. Baird, *Organometallics* **2017**, *36*, 3508.

[21] X. Li, J. Zhang, Y. Zhao, X. Zhao, F. Li, T. Li, H. L. Li, L. Chen, *J. Mater. Chem. A* **2015**, *3*, 6265.

[22] L.-X. You, H.-J. Liu, L.-X. Cui, F. Ding, G. Xiong, S.-J. Wang, B.-Y. Ren, I. Dragutan, V. Dragutan, Y.-G. Sun, *Dalton Trans.* **2016**, *45*, 18455.

[23] J.-Y. Song, X. Zhou, H. Song, Y. Liu, H.-Y. Zhao, Z.-Z. Sun, W.-Y. Chu, *ChemCatChem* **2018**, *10*, 758.

[24] F. Kreyenschmidt, K. Koszinowski, *Chem. – Eur. J.* **2018**, *24*, 1168.

[25] P. M. P. Garcia, T. D. Franco, A. Epenoy, R. Scopelliti, X. Hu, *ACS Catal.* **2016**, *6*, 258.

[26] J. M. Neely, M. J. Bezdek, P. J. Chirik, *ACS Cent. Sci.* **2016**, *2*, 935.

[27] H. M. Abd El-Lateef, V. M. Abbasov, L. I. Aliyeva, M. M. Khalaf, *Egypt. J. Pet.* **2015**, *24*, 175.

[28] H. M. Abd El-Lateef, V. M. Abbasov, L. I. Aliyeva, E. E. Qasimov, I. T. Ismayilov, *Mater. Chem. Phys.* **2013**, *142*, 502.

[29] H. M. Abd El-Lateef, *Corros. Sci.* **2015**, *92*, 104.

[30] E. A. Noor, A. H. Al-Moubaraki, *Mater. Chem. Phys.* **2008**, *110*, 145.

[31] O. A. M. Ali, *Spectrochim. Acta A* **2014**, *132*, 52.

[32] M. Das, A. Biswas, B. K. Kundu, S. M. Mobin, G. Udayabhanu, S. Mukhopadhyay, *RSC Adv.* **2017**, *7*, 48569.

[33] E. Yousif, E. Bakir, J. Salimon, N. Salih, *J. Saudi Chem. Soc.* **2012**, *16*, 279.

[34] M. S. S. Adam, H. M. Abd El-Lateef, K. A. Soliman, *J. Mol. Liq.* **2018**, *250*, 307.

[35] M. Enamullah, M. A. Quddus, M. M. Rahman, T. E. Burrow, *J. Mol. Struct.* **2017**, *1130*, 765.

[36] M. S. S. Adam, *Monatsh. Chem.* **2015**, *146*, 1823.

[37] M. S. S. Adam, *Appl. Organomet. Chem.* **2018**, *32*, e4234.

[38] H. M. Abd El-Lateef, M. S. S. Adam, M. M. Khalaf, *J. Taiwan Inst. Chem. Eng.* **2018**, *88*, 286.

[39] M. S. S. Adam, A. D. M. Mohamad, *Polyhedron* **2018**, *151*, 118.

[40] P. Job, *Ann. Chem.* **1928**, *9*, 113.

[41] V. Ramakrishna, N. D. Reddy, *Dalton Trans.* **2017**, *46*, 8598.

[42] A. J. J. Lennox, G. C. Lloyd-Jones, *Chem. Soc. Rev.* **2014**, *42*, 412.

[43] E. L. Kolychev, A. F. Asachenko, P. B. Dzhevakov, A. A. Bush, V. V. Shuntikov, V. N. Khrustalevc, M. S. Nechaev, *Dalton Trans.* **2013**, *42*, 6859.

[44] F. Kong, C. Zhou, J. Wang, Z. Yu, R. Wang, *ChemPlusChem* **2013**, *78*, 1.

[45] S. Fortun, P. Beauclair, A. R. Schmitzer, *RSC Adv.* **2017**, *7*, 21036.

[46] C. A. Fleckenstein, H. Plenio, *Chem. – Eur. J.* **2007**, *13*, 2701.

[47] Y. Sunesson, E. Limé, S. O. N. Lill, R. E. Meadows, P.-O. Norrby, *J. Org. Chem.* **2014**, *79*, 11961.

[48] H. Shi, W. Dai, B. Wang, S. Cao, *Organometallics* **2018**, *37*, 459.

[49] M. T. Quiros, D. Collado-Sanz, E. Bunuel, D. J. Cardenas, *J. Phys. Chem. A* **2018**, *122*, 2250.

[50] T. Korenaga, K. Abe, A. Ko, R. Maenishi, T. Sakai, *Organometallics* **2010**, *29*, 4025.

[51] H. Xu, J. B. Diccianni, J. Katigbak, C. Hu, Y. Zhang, T. Diao, *J. Am. Chem. Soc.* **2016**, *138*, 4779.

[52] T. Hirakawa, Y. Uramoto, S. Yanagisawa, T. Ikeda, K. Inagaki, Y. Morikawa, *J. Phys. Chem. C* **2017**, *121*, 19904.

[53] V. I. Bakhmutov, F. Bozoglian, K. Gómez, G. González, V. V. Grushin, S. A. Macgregor, E. Martin, F. M. Miloserdov, M. A. Novikov, J. A. Panetier, L. V. Romashov, *Organometallics* **2012**, *31*, 1315.

[54] X. Li, Z. Feng, Z.-X. Jiang, X. Zhang, *Org. Lett.* **2015**, *17*, 5570.

[55] E. J. Tollefson, L. W. Erickson, E. R. Jarvo, *J. Am. Chem. Soc.* **2015**, *137*, 9760.

[56] P.-A. Payard, L. A. Perego, I. Ciofini, L. Grimaud, *ACS Catal.* **2018**, *8*, 4812.

[57] M. García-Melchor, A. A. C. Braga, A. Lledós, G. Ujaque, F. Maseras, *Acc. Chem. Res.* **2013**, *46*, 2626.

[58] R. K. Rai, K. Gupta, D. Tyagi, A. Mahata, S. Behrens, X.-C. Yang, Q. Xu, B. Pathakad, S. K. Singh, *Catal. Sci. Technol.* **2016**, *6*, 5567.

[59] K. P. Ansari, M. A. Quraishi, A. Singh, *Corros. Sci.* **2014**, *79*, 5.

[60] V. V. Torres, V. A. Rayol, M. Magalháes, G. M. Viana, L. C. S. Aguiar, S. P. Machado, E. D'Elia, *Corros. Sci.* **2014**, *79*, 108.

[61] B. G. Zhang, C. J. He, X. Chen, Z. P. Tian, F. T. Li, *Corros. Sci.* **2015**, *90*, 585.

[62] H. Bentrah, Y. Rahali, A. Chala, *Corros. Sci.* **2014**, *82*, 426.

[63] N. Soltani, N. Tavakkoli, M. Khayatkashani, M. R. Jalali, A. Mosavizade, *Corros. Sci.* **2012**, *62*, 122.

[64] Y. Qiang, S. Zhang, S. Xu, L. Yin, *RSC Adv.* **2015**, *5*, 63866.

[65] E. Gutiérrez, J. A. Rodríguez, J. Cruz-Borbolla, J. G. Alvarado-Rodriguez, P. Thangarasu, *Corros. Sci.* **2016**, *108*, 23.

[66] L. Luo, S. T. Zhang, Y. Qiang, *Int. J. Electrochem. Sci.* **2016**, *11*, 8177.

[67] M. Mishra, K. Tiwari, P. Mourya, M. M. Singh, V. P. Singh, *Polyhedron* **2015**, *89*, 29.

[68] A. M. Nassar, A. M. Hassan, M. A. Shoeib, A. N. El Kmash, *J. Bio. Tribo. Corros.* **2015**, *19*, 1.

[69] F. Bentissa, M. Traisnelb, M. Lagrenee, *Corros. Sci.* **2000**, *42*, 127.

[70] A. Pandey, B. Singh, C. Verma, E. E. Ebenso, *RSC Adv.* **2017**, *7*, 47148.

[71] R. Solmaza, G. Kardas, M. Çulha, B. Yazıcı, M. Erbil, *Electrochim. Acta* **2008**, *53*, 5941.

[72] R. Solmaz, *Corros. Sci.* **2010**, *52*, 3321.

[73] C. Verma, M. A. Quraishi, E. E. Ebenso, I. B. Obot, A. El Assyry, *J. Mol. Liq.* **2015**, *218*, 647.

[74] H. M. Abd El-Lateef, A. H. Tantawy, *RSC Adv.* **2016**, *6*, 8681.

[75] H. M. Abd El-Lateef, M. A. Abo-Riya, A. H. Tantawy, *Corros. Sci.* **2016**, *108*, 94.

[76] M. Lagrenee, B. Mernari, M. Bouanis, M. Traisnel, F. Bentiss, *Corros. Sci.* **2002**, *44*, 573.

[77] M. T. Alhaffar, S. A. Umoren, I. B. Obot, S. A. Ali, *RSC Adv.* **2018**, *8*, 1764.

[78] M. A. Chidiebere, E. E. Oguzie, L. Liu, Y. Li, F. Wang, *Ind. Eng. Chem. Res.* **2014**, *53*, 7670.

[79] M. A. Bedair, M. M. B. El-Sabbah, A. S. Fouda, H. M. Elaryian, *Corros. Sci.* **2017**, *128*, 54.

[80] M. Bouanis, M. Tourabi, A. Nyassi, A. Zarrouk, C. Jama, F. Bentiss, *Appl. Surf. Sci.* **2016**, *389*, 952.

[81] M. Mobin, S. Zehra, R. Aslam, *RSC Adv.* **2016**, *6*, 5890.

[82] K. R. Ansari, M. A. Quraishi, A. Singh, *Corros. Sci.* **2015**, *95*, 62.

[83] H. T. M. Abdel-Fatah, M. M. Kamel, A. A. M. Hassan, S. A. M. Rashwan, S. M. Abd El Wahaab, H. E. E. El-Sehiety, *Arab. J. Chem.* **2017**, *10*, S1164.

[84] C. Chai, Y. Xu, S. Shi, X. Zhao, Y. Wu, Y. Xu, L. Zhang, *RSC Adv.* **2018**, *8*, 24970.

[85] A. Kosari, M. H. Moayed, A. Davoodi, R. Parvizi, M. Momeni, H. Eshghi, H. Moradi, *Corros. Sci.* **2014**, *78*, 138.

SUPPORTING INFORMATION

Additional supporting information may be found online in the Supporting Information section at the end of the article.

How to cite this article: Abd El-Lateef HM, Sayed AR, Adam MSS. Sulfonated salicylidene thiadiazole complexes with Co (II) and Ni (II) ions as sustainable corrosion inhibitors and catalysts for cross coupling reaction. *Appl Organometal Chem*. 2019;e4987. https://doi.org/10.1002/aoc.4987